AIAA JOURNAL
Vol. 32, No. 7, July 1994

Vortex Cutting by a Blade, Part II: Computations of Vortex Response

J. S. Marshall*
University of Iowa, Iowa City, Iowa 52242
and
R. Yalamanchili†
Florida Atlantic University, Boca Raton, Florida 33431

Computations of the interaction between a line vortex and blades of various thicknesses and angles of attack traveling in a direction normal to the vortex axis have been performed. A procedure to enable instantaneous cutting of the vortex is used in the case of thin blades to study vortex interaction with the blade both before and after vortex cutting has occurred. To isolate the effect of blade thickness on vortex bending, additional computations have been performed of the interaction between a line vortex and circular cylinders of various diameters. The vortex is represented by a filament model which includes axial flow within the core and nonuniform core area, and the effect of the blade or cylinder on the vortex is obtained using a vortex sheet panel method. The study particularly examines bending of the vortex and the subsequent variation in vortex core radius. It is found that the amount of vortex bending is primarily dependent on the ratio of blade thickness T (or diameter D of a circular cylinder) to ambient vortex core radius σ_o. For blades with T/σ_o of order unity or less, very little bending is observed for attack angles under the stall limit. For cases in which significant vortex bending is observed (T/σ_o or D/σ_o greater than order unity), increase in blade or cylinder forward speed results in a decrease in vortex core radius for a given amount of bending of the vortex axis. Vortex shocks and expansion waves are also observed to propagate on the vortex after cutting by a blade, as predicted in Part I of the study.[1]

I. Introduction

THIS paper reports on a computational study of the problem of normal blade-vortex interaction, including cutting of the vortex by the blade. We are particularly interested in examining the degree of bending of the vortex both prior to and following cutting, which has implications on the extent of applicability of a simple analytical solution of the problem given in Part I of the study.[1] In this solution, it is predicted that cutting of a vortex will cause the formation of a vortex shock and a vortex expansion wave on opposite sides of the blade, both of which propagate on the vortex away from the blade. The expansion wave causes a gradual decrease of core radius, whereas the vortex shock is typified by an abrupt increase in core radius as it propagates past a material section of the vortex core. It is noted that we are dealing with an incompressible fluid in this paper, and that terms such as vortex "shock" and "expansion wave" are used only because of the similarity between the equations governing axial motion on the vortex core and the one-dimensional gas dynamics equations.[1] For thin blades which cut the vortex, the force on the blade depends mainly on the ratio of the vortex core radius on opposing sides of the blade. Suction of fluid from the blade boundary layer into the vortex contributes an additional force on the blade, but this effect seems to be weak.

The analytical solution in Part I is based on the assumption that the vortex axis is nearly straight, or rather that the blade does not cause a significant amount of bending of the vortex. Vortex bending, were it to occur, would cause a stretching of the vortex near the blade and a local decrease in core radius. In the present paper, a computational study of vortex interaction with a blade is performed to determine the amount of bending that occurs for various angles of attack of the blade and ratios of blade thickness to core radius and of blade forward speed to vortex azimuthal velocity. The computations (which are based on the long-wave theory derived in Part I) consider the evolution of the vortex both before and after cutting (which is assumed to occur instantaneously) and include both lateral deflection of the vortex and axial flow (including vortex shocks) within the core. Computations have also been performed for vortex bending by circular cylinders, which is somewhat simpler than the vortex-blade interaction problem and isolates the effect of blade thickness.

Although the problem of vortex response due to normal interaction with a blade does not seem to have been previously studied in detail, a number of computational studies have considered vortex bending by close interaction with bodies of other shapes, including a sphere[2,3] and a circular cylinder.[4] In Ref. 2, an analytical solution for small deflection of the vortex by a stationary sphere is also given. There are a number of both theoretical and experimental studies of other aspects of the normal blade-vortex interaction problem, dealing with blade pressure fluctuations and sound generation, which are discussed in Part I. An experimental investigation of the interaction of a rotor tip vortex and a large-diameter cylinder was performed by Liou et al.[5]; however, the flow visualization technique used in this study to determine the vortex response fails for close interactions of the vortex with the cylinder surface and after the interaction with the cylinder has occurred. These previous studies generally consider bodies which are much thicker than the vortex core (so that a substantial amount of bending occurs), and the computational studies do not allow the vortex to be cut by the body and do not include a prediction of axial flow within the vortex core and variation of the core area.

We note that in a purely inviscid theory, as is assumed in the present paper, the vortex would wrap around the blade and cutting of the vortex could never occur. Vortex cutting, like vortex reconnection, is dependent on the presence of fluid viscosity for it to occur; however, we assume that the gross details of vortex cutting, including prediction of its occur-

Received June 29, 1993; revision received Nov. 16, 1993; accepted for publication Nov. 30, 1993.

*Associate Professor, Iowa Institute of Hydraulic Research.
† Graduate Research Assistant, Department of Ocean Engineering.

rence, is not dependent on the value of the viscosity (as seems to be the case with vortex reconnection problems in general). We do not investigate the cutting process itself in the present paper, but rather we employ a procedure for instantaneous cutting of the vortex to investigate the motion of the vortex both before and after cutting.

The numerical method used in the computations is described in Sec. II. of the paper, including the procedure used to produce vortex cutting. The results of computations for vortex-blade interaction, including cutting of the vortex, are described in Sec. III. We examine in this section the influence of blade angle of attack, thickness and forward speed and vortex core radius, circulation, and axial flow rate on the bending of the vortex both before and after cutting. Results for interaction of a vortex and circular cylinders of various diameters are described in Sec. IV., followed by some conclusions in Sec. V.

II. Numerical Method

In the numerical simulation of the interaction and cutting of a vortex by a blade, the vortex is represented by a filament model which allows variable core area and axial flow (derived in Part I), and the boundary layer on the surface of the blade is represented by a vortex sheet. The vortex filament occupies a space curve C, and the position vector to a material point ξ on C relative to a fixed coordinate system is denoted by $r = r(\xi, t)$. The blade surface occupies a space surface S, and the position vector of a material point (η, ϕ) on S is denoted by $x = x(\eta, \phi, t)$. Here ξ, η, and ϕ are Lagrangian coordinates which are constant at any material point for all time. The vortex circulation is denoted by Γ and the vortex sheet strength on S is denoted by $\gamma(\eta, \phi, t)$.

A Lagrangian approach is used for the numerical computation, where at every time step we solve for the central position r of a segment with control point ξ on the vortex filament C and the strength γ of a panel with control point (η, ϕ) on the vortex sheet on S. The motion of the vortex filament is calculated using the long-wave theory derived in Part I, which yields equations for the velocity components u, v, and w of a point ξ in the principal normal, binormal, and tangential directions to C, respectively, as

$$u = u_I + u_E, \quad v = v_I + v_E + \frac{\kappa\Gamma}{16\pi} - \frac{\pi\sigma^2\kappa w_A^2}{\Gamma}$$
$$w = w_A + w_I + w_E \tag{1}$$

where $\sigma = \sigma(\xi, t)$ is the vortex core radius, (u_I, v_I, w_I) are the components of the self-induced velocity of the vortex, (u_E, v_E, w_E) are the external velocity components due to interaction with the blade and $w_A = w_A(\xi, t)$ is an additional axial velocity given by solution of the differential equation

$$\sigma^2\dot{w}_A = -\frac{\Gamma^2}{4\pi^2\sigma}\frac{\partial\sigma}{\partial s} \tag{2}$$

Here the superposed dot represents the material time derivative and s is a measure of arc length along C determined from

$$ds = |\partial r/\partial\xi|\, d\xi \tag{3}$$

The core radius σ is determined from the continuity equation for the vortex core, given by

$$\sigma^2(\partial s/\partial\xi) = \text{const} \tag{4}$$

The unit vectors $(\lambda_1, \lambda_2, \lambda_3)$ in the principal normal, binormal, and tangential directions and the curvature κ can be determined from the position vector $r(\xi, t)$ of C using Eqs. (4–8) of Part I. The self-induced velocity u_I and external interaction velocity u_E are obtained from the Biot-Savart integral, with the Rosenhead regularization of the singularity in the integral over C, giving

$$u_I(\xi, t) = -\frac{\Gamma}{4\pi}\int_C \frac{[r(\xi, t) - r(\xi', t)]}{\{|r(\xi, t) - r(\xi', t)|^2 + \mu^2(\xi, t)\}^{3/2}} \times \frac{dr}{d\xi}(\xi', t)\, d\xi' \tag{5a}$$

$$u_E(\xi, t) = -\frac{1}{4\pi}\int_S \frac{[r(\xi, t) - x(\eta, \phi, t)]}{|r(\xi, t) - x(\eta, \phi, t)|^3} \times \gamma(\eta, \phi, t)\, da(\eta, \phi) \tag{5b}$$

where da is an infinitesimal area on S and $\mu(\xi, t) = 2\delta_R\sigma(\xi, t)$. As discussed in Part I, even though the calculations presented here apply to vortices with uniform vorticity profile within each cross section of the core, the cut-off constant δ_R is chosen as that appropriate for a hollow core vortex, or $\delta_R = (1/2)\exp(-1/2)$, as the internal forces within the core are accounted for by the last two terms in the second equation in Eq. (1). Using Eqs. (1–5), the vortex velocity components (u, v, w) and core radius σ can be determined given the position $r(\xi, t)$ of points ξ on C, a solution for the axial flow rate w_A from Eq. (2), the location x of the blade surface S, and the strength γ of the vortex sheet on S.

The motion of the blade surface S is specified by

$$\frac{dx}{dt} = -Ue_x \tag{6}$$

where U is the blade forward speed and e_x is the base vector in the x direction. We now let (i_1, i_2, i_3) denote orthogonal unit vectors on S, such that i_3 is everywhere normal to S and i_1 and i_2 are everywhere parallel to S. All three vectors (i_1, i_2, i_3) vary with η and ϕ, but are independent of time. The vortex sheet strength γ on S can then be determined from the boundary condition on S by solution of[6]

$$i_3 \times \left[\left(w_I + w_E - \frac{dx}{dt}\right) \times i_3\right] = -\frac{1}{2}\gamma \times i_3 \tag{7}$$

where w_I is the self-induced velocity of the vortex sheet, w_E is the induced velocity on S due to the vortex filament, and dx/dt is the blade velocity given by Eq. (6). The left-hand side of Eq. (7) is the projection on a plane tangent to S at (η, ϕ) of the difference between the inviscid slip velocity at a point just above S (due to both induced velocity from the vortex filament and from distant parts of the sheet) and the blade velocity. The right-hand side of Eq. (7) is one half of the jump in velocity over the vortex sheet, the other half being provided by the local contribution to w_I. The no-penetration condition on S is identically satisfied by solutions of Eq. (7). Expressions for w_I and w_E are obtained from the Biot-Savart equation, again applying the Rosenhead cutoff for the integration over C, as

$$w_I(\eta, \phi, t) = -\frac{1}{4\pi}\int_S \frac{[x(\eta, \phi, t) - x(\eta', \phi', t)]}{|x(\eta, \phi, t) - x(\eta', \phi', t)|^3} \times \gamma(\eta', \phi', t)\, da(\eta', \phi') \tag{8a}$$

$$w_E(\eta, \phi, t) = -\frac{\Gamma}{4\pi}\int_C \frac{[x(\eta, \phi, t) - r(\xi', t)]}{\{|x(\eta, \phi, t) - r(\xi', t)|^2 + \mu^2(\xi, t)\}^{3/2}} \times \frac{dr}{d\xi}(\xi', t)\, d\xi' \tag{8b}$$

where the $\mu(\xi, t)$ is related to the core radius $\sigma(\xi, t)$ of the closest point on C to the point (η, ϕ) on S by $\mu = 2\delta_R\sigma$ and $\delta_R = (1/2)\exp(-1/2)$ as given previously following Eq. (6). We note that the kernels of the integrals in Eqs. (5b) and (8a) are singular; however, the singularities are integrable. Equa-

tions (7–8b) yield an integral equation for γ for given values of x and r.

During the numerical computations, the curve C is discretized into segments and the surface S is discretized into panels. The initial condition for C is a straight line, but the segments are shorter near the central portion of C than they are near the ends. The integration over C is only carried out to a distance $|\xi| = A$. To account for the induced velocity from the sections of the vortex extending infinitely above and infinitely below the points $\xi = \pm A$, we use a procedure suggested by Dhanak[2] in which the integration over C in Eqs. (5a) and (8b) is understood to imply integration only over the interval $|\xi| < A$ and the integration over the region $|\xi| \geq A$ is performed analytically assuming that the vortex axis is straight in these regions. This procedure yields an extra term $\boldsymbol{I}$ which is added to the right-hand sides of Eqs. (5a) and (8b), given by

$$\boldsymbol{I} = \frac{\Gamma}{4\pi} \frac{\boldsymbol{e}_y \times \boldsymbol{s}}{|\boldsymbol{s}|^2} \left[2 - \frac{A - \boldsymbol{s} \cdot \boldsymbol{e}_y}{|\boldsymbol{s} - A\boldsymbol{e}_y|} - \frac{A + \boldsymbol{s} \cdot \boldsymbol{e}_y}{|\boldsymbol{s} + A\boldsymbol{e}_y|} \right] \tag{9}$$

where the vortex axis coincides with the coordinate axis $\boldsymbol{e}_y$ for $|\xi| > A$ and the vector $\boldsymbol{s}$ is given by $\boldsymbol{r}(\xi, t)$ in Eq. (5a) and by $\boldsymbol{x}(\eta, \phi, t)$ in Eq. (8b). The parameter μ has been dropped in Eq. (9) because $|\boldsymbol{s}| \gg \sigma$ everywhere.

Differentiation along the vortex filament with respect to ξ is performed using three-point central difference formulas for nonuniform grid spacings, and the integrals over C are performed using the trapezoidal rule. The integration over S in Eqs. (5b) and (8a) is also performed using the trapezoidal rule for all panels except that containing the point (η, ϕ), at which the kernel is singular. Over this panel, the integration is performed analytically with the assumption that the sheet strength γ is uniform. The panels are also of nonuniform sizes, such that thinner panels are used near the leading and trailing edges of the blade and the panels are more concentrated near the vortex in the spanwise (z) direction. The results presented here are for 400 segments along the vortex and 600 panels on the blade, with 20 control points along the blade span and 30 along the chord.

A perspective view showing the panels on the blade and the segments of the vortex (showing only every other segment) in the initial configuration is given in Fig. 1. The spacing between segments on the vortex is half as long in the region near the blade as it is in the regions distant from the blade. The panel spacing on the blade is also closer near the leading edge and near the center, where the blade comes in close interaction with the vortex. The initial distance between the blade leading edge and the vortex axis was set to one half of the blade chord for the runs with vortex-blade interaction and ten times the vortex core radius for runs with vortex-cylinder interaction. A schematic showing the blade and vortex axis orientation in terms of the global Cartesian coordinate system $(\boldsymbol{e}_x, \boldsymbol{e}_y, \boldsymbol{e}_z)$ and the blade surface coordinate system $(\boldsymbol{i}_1, \boldsymbol{i}_2, \boldsymbol{i}_3)$ is given in Fig. 2.

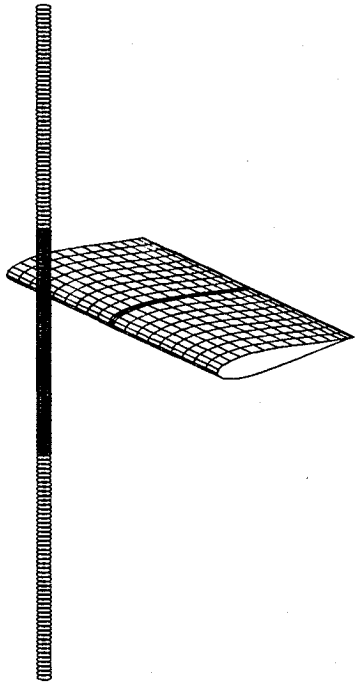

Fig. 1 Plot showing the panels on the blade surface and the segments on the vortex (with only every second segment plotted) at the initial time from a perspective view.

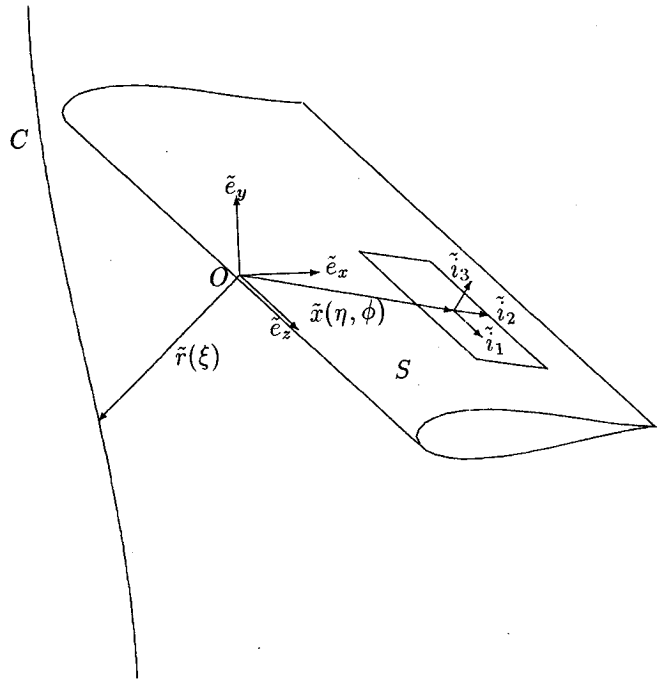

Fig. 2 Schematic showing the orientation of the Cartesian base vectors $(\boldsymbol{e}_x, \boldsymbol{e}_y, \boldsymbol{e}_z)$ and curvilinear base vectors $(\boldsymbol{i}_1, \boldsymbol{i}_2, \boldsymbol{i}_3)$ on the blade surface with respect to the blade surface S and the vortex axis C.

The panels on the blade extend in the spanwise direction to points $z = \pm L$. Rather than trying to compute a blade of finite span (which would require inclusion of tip vortices from the blade), we employ periodic boundary conditions in the z direction at $z = \pm L$, with two reflections on each side of the entire flowfield within $|z| < L$ (see also Ref. 6). The Kutta condition is enforced by requiring that the spanwise component of the vortex sheet strength $\gamma^+ \cdot \boldsymbol{e}_z$ on the upper side of the blade at the trailing edge be equal to the negative of the spanwise component $\gamma^- \cdot \boldsymbol{e}_z$ of the sheet strength on the lower side of the blade at the trailing edge.[6]

Time stepping is carried out using a two-step predictor-corrector method. A solution for w_A from Eq. (2) is obtained by writing the right-hand side of Eq. (2) in conservative form and using MacCormack's method,[7] in which forward differencing is performed on the predictor step and backward differencing is performed on the corrector step. Following cutting of the vortex, it is found that use of a second-order upwind scheme for the solution of Eq. (2) gives the best resolution of the vortex shock. The time step (set in all of the calculations presented in the paper at $\Gamma \Delta t / 2\pi\sigma_o^2 = 0.2$) is smaller than that required by the Courant-Friedrichs-Lewy condition for stability of MacCormack's scheme in all cases by a factor of at least 10. The boundary condition $w_A = w_o$ is enforced at the upstream end of the vortex filament prior to cutting of the vortex.

Vortex cutting is performed instantaneously when the blade leading edge extends into the core and is within some small fraction f of the initial core radius from the vortex axis. In the computations we selected $f = 0.25$, although the results do not

seem to be particularly sensitive to the choice of f. The cutting is achieved by translating the blade a small distance $R \simeq 2f$ in the negative x direction with the vortex filament frozen and then deleting the section of the vortex that lies within the blade in its new position. To complete the cutting, two new control points are generated at the points where the vortex intersects the blade surface in the translated position. After cutting, the motion of the two sections of the vortex is solved for separately. In the present paper it is assumed that there is no suction of the blade boundary-layer fluid into the vortex, so we set $w_A = 0$ at points where the vortex intersects the blade. Other boundary conditions on w_A are also possible, however, such as the formula for vortex suction given in Part I.

Some additional measures were used to improve the accuracy of the solution after cutting. One of these measures follows from the observation that the segment length on C is generally much shorter than the panel width on S, so that evaluation of the kernel of the integral in Eq. (5b) to determine the induced velocity on the vortex filament from the vortex sheet is not very accurate for sections of the vortex very close to the blade. To correct this problem, we subdivide the panel at which the vortex filament intersects the blade and its neighboring panels, each into some number (typically about 40) of subpanels, where the vortex sheet strength of the subpanels is equal to that of the main panel.

Secondly, as predicted by the solution in Part I, a vortex shock will generally form on the vortex following cutting by the blade (for nonzero vortex axial flow or blade angle of attack). As this shock propagates past a point on the filament, the core radius associated with that point abruptly increases, sometimes by a large amount. As the stretch of the vortex axis is inversely proportional to the core radius squared [see Eq. (4)], passage of a strong shock may cause quite a substantial and abrupt compression of the control points along C. In a Lagrangian calculation, it is sometimes necessary to make the time step very small to accurately capture this compression, even though the strength of the vortex sheet on S and the lateral deflection of C (determination of which together consumes the vast majority of the computational time) do not change much over this integral. To speed up the computations while still maintaining accuracy, we utilize two separate time steps after cutting occurs. The short time step is used to determine the change in core radius and axial motion of the control points on the filament, and the large time step is used to determine the change in strength of the vortex sheet and the lateral deflection of the vortex. In the current computations, the short time step was chosen to be 10 times smaller than the long time step. A predictor-corrector algorithm is used with both time steps.

As discussed by Peyret and Taylor,[7] spurious oscillations are commonly observed near shocks in numerical calculations of the gas dynamics equations with shock-capturing schemes (such as MacCormack's method). An accurate solution for the shock can be obtained by suppressing these oscillations with a viscous filter,[7] which in the calculations for w_A takes the form

$$w_A(\xi) = \bar{w}_A(\xi) + \nu[\bar{w}_A(\xi + \Delta\xi) - 2\bar{w}_A(\xi) + \bar{w}_A(\xi - \Delta\xi)] \quad (10)$$

such that the overbar denotes unfiltered values of the axial flow rate and $\nu(\Delta\xi)^2$ is dimensionless numerical viscosity. In the current calculations, ν was set equal to 0.01, which was found to eliminate the numerical oscillations without significantly affecting the axial flow in other regions of the vortex.

Testing of the code accuracy and of the choice of the various computational parameters is discussed in the thesis of Yalamanchili.[8] The calculation of vortex self-induced velocity was tested by comparison to the results of Dhanak and DeBernardinis[9] for oscillatory motion of an elliptical vortex ring, for which an approximate analytical solution exists for small ellipse aspect ratios. The calculation of flow past the blade was tested by comparison to the exact solution for a steady two-dimensional potential flow (with no vortex). The choice of computational parameters (such as the time step) was tested both by comparing to the exact solutions, and by repeating calculations with the value of a given parameter reduced or increased, and noting negligible change in the results.

III. Results for Vortex-Blade Interactions

In this section, we report the results of computations of the interaction and cutting of a vortex by blades of various thicknesses. The blade shape was given by a Joukowski airfoil with a chord length of 30 times the ambient vortex core radius. Computations are first presented for very thin blades, with $T/\sigma_o \leq 0(1)$, and the effect of blade thickness is then estimated by repeating these computations with progressively thicker blades. The behavior of the vortex for thin and thick blades, as determined by the ratio T/σ_o of blade thickness to ambient core radius, is qualitatively different, as will be demonstrated hereafter.

For the case of thin blades [such that $T/\sigma_o \leq 0(1)$], the vortex is observed not to bend substantially during interaction with the blade, either before or after cutting. An example of such a case, shown just after cutting, is given for a thin blade at zero angle of attack in Fig. 3. For the case shown, the dimensionless blade thickness, axial flow rate, and blade forward speed are given by $T/\sigma_o = 1/2$, $2\pi\sigma_o w_o/\Gamma = -1/2$, and $2\pi\sigma_o U/\Gamma = 1$, respectively. In the figure, a circle is drawn about the vortex core at Lagrangian control points (where only every other control point is used). For the part of the vortex axis shown in Fig. 1 the segments along the core are initially of uniform length. On the upper side of the vortex (above the blade), a vortex shock is found to occur, such that the core is compressed axially and the vortex core is increased near the blade. On the lower side of the vortex (below the blade), a vortex expansion wave occurs, such that the vortex expands axially and the core radius decreases near the blade. The asymmetry in the vortex response in Fig. 1 is due to the effect of the ambient axial flow, which compresses the core along its axis on the upper side and expands it on the lower side of the blade. A plot of core radius vs vertical distance is given in Fig. 4 for the same case as shown in Fig. 3. The sudden jump in core radius in Fig. 4 occurs when the blade intersects the vortex. As the computation progresses in time, the vortex shock propagates upward away from the blade and

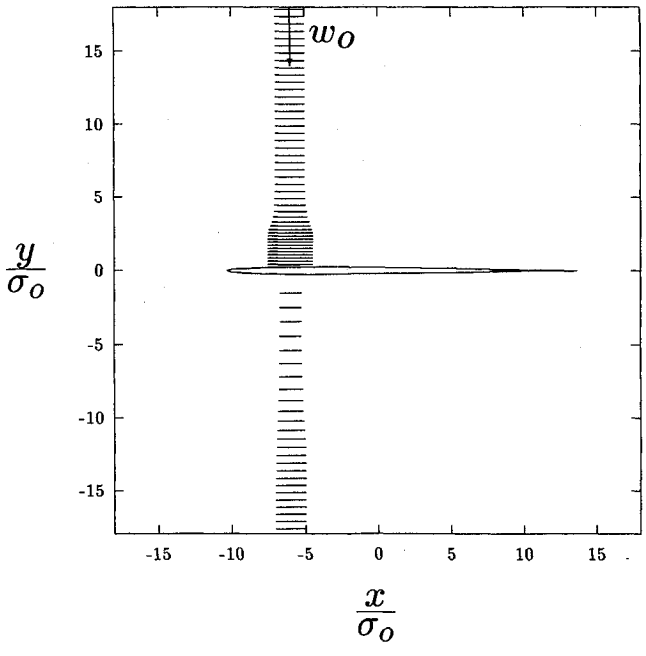

Fig. 3 Side view (looking along the blade span) of a vortex with axial flow rate $2\pi w_o \sigma_o/\Gamma = -1/2$ after cutting by a blade with angle of attack $\alpha = 0$ deg, forward speed $2\pi U\sigma_o/\Gamma = 1$, and thickness $T/\sigma_o = 1$; a shock forms on the vortex above the blade and an expansion wave forms on the vortex below the blade.

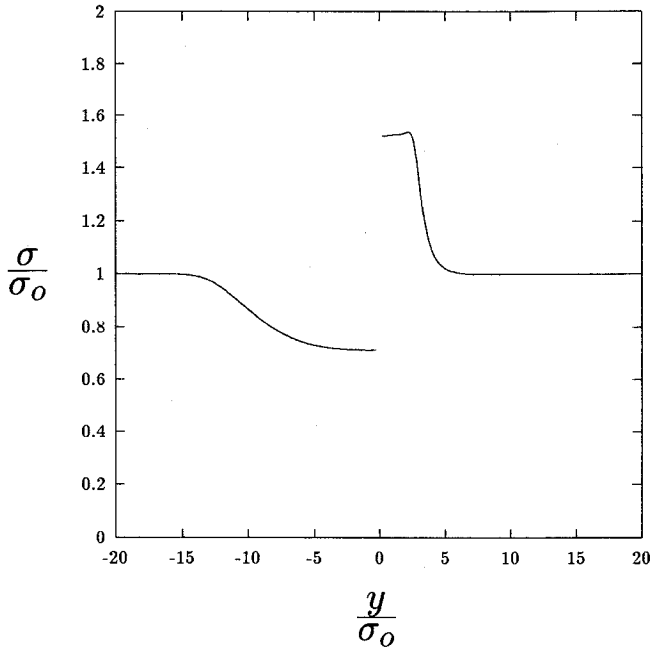

Fig. 4 Variation of vortex core radius σ with distance along the vortex for the same run and at the same time as shown in Fig. 3; the blade cuts the vortex at the position of the jump in σ.

the expansion wave elongates and propagates downward away from the blade.

The vortex force on the blade is calculated as a function of time, both before and after cutting, by integrating the product of the pressure acting on each panel and the inward unit normal $-i_3$ over S, and then subtracting the force on the blade in the absence of the vortex. Following cutting, the pressure within the vortex core is not included in the force calculation because, as was noted in Part I, the net force exerted by the interior of the vortex core is the same on both sides of the blade (even if the core radii on the two sides are different). The pressure is computed by approximating the velocity relative to the blade at a point on the blade surface S by the vortex sheet strength γ at that point, so that Euler's equation gives

$$\frac{\partial}{\partial s}\left(p + \frac{\rho}{2}\gamma\cdot\gamma\right) + \rho\frac{\partial\gamma}{\partial t} = 0 \tag{11}$$

where the vector s measures length along the blade surface S. Letting (s_1, s_2) be the components of s along the (i_1, i_2) directions, where i_1 points along the blade span and i_2 lies in the cross-sectional plane of the blade, we integrate Eq. (11) over s_1 to obtain

$$p(s_1, s_2, t) = -\frac{\rho}{2}|\gamma(s_1, s_2, t)|^2 - \int_0^{s_1}\rho\frac{\partial\gamma_1}{\partial t}(s_1', s_2, t)\,ds_1' + C(s_2, t) \tag{12}$$

As p approaches the solution for two-dimensional flow past a blade far away from the vortex, the function C in Eq. (12), which is independent of s_1, must not contribute to the vortex force on the blade.

A plot of the variation with time of the magnitude F_B of vortex force on the blade is given in Fig. 5 for a numerical computation (solid curve) with $\alpha = 0$ deg (for the same values of parameters as the case in Fig. 3). The vortex exerts very little force on the blade prior to cutting, and the force computed after cutting is close to that obtained analytically in Part I (dashed curve). The wiggles on the curve in Fig. 5 for the numerical prediction of force occur only for cases in which vortex cutting has occurred, and are due to the vortex core passing over panels on the blade surface. The sudden change in vortex force at the instant of cutting would thus seem to be primarily responsible for sound production during vortex interaction with thin blades. As the actual cutting of the vortex is assumed to occur instantaneously, the present calculations cannot address the possibility that the vortex force on the blade may not vary monotonically from its value before cutting to that just after cutting (i.e., that there may be a spike in vortex force just at the instant of cutting). This point should be examined further in future work.

A variety of runs with thin blades with nonzero angle of attack and various blade speeds have also been performed, and we again observe very little bending of the vortex either prior to, or after cutting, and very little change in vortex force on the blade before cutting. Our results therefore generally indicate that for T/σ_o less than about unity, the vortex behavior closely follows the analytical solution given in Part I.

For blades which are thick compared to the vortex core radius, substantial bending can occur without vortex cutting, such that at some later time the vortex core radius is substantially reduced near the blade and the vortex axis lies nearly parallel to the blade surface. An example of this behavior is shown in Fig. 6 for a case with $T/\sigma_o = 5$, $2\pi\sigma_o U/\Gamma = 1$ and no ambient axial flow. In this figure, we observe that the vortex bends around the blade at the leading edge, such that the blade does not penetrate the vortex core. As described in the next section, the vortex behavior in this case is very similar to that which occurs during the interaction of a vortex and a circular cylinder with an equivalent value of D/σ_o.

Very substantial bending of the vortex is observed for cases with a thick blade at a fairly large angle of attack. For instance, in Fig. 7 the same case is shown as in Fig. 6, but with $\alpha = -15$ deg. We observe that the vortex forms a kink just below the blade, near the leading edge, well before the blade leading edge comes into close contact with the vortex. A series of curves showing the variation of core radius with vertical distance at several different time steps is given in Figs. 8 and 9 for the same two cases shown in Figs. 6 and 7, respectively. The curves in Fig. 8 are plotted every 10 time steps and those in Fig. 9 are plotted every 5 time steps. For the case with a zero angle of attack in Fig. 8, the core radius decreases somewhat as it is stretched by the blade leading edge. For the case with

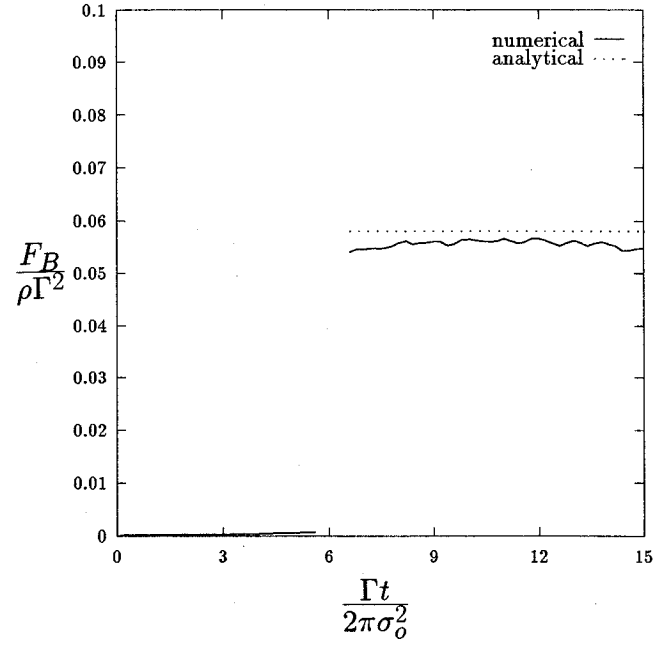

Fig. 5 Magnitude of the vortex force F_B on the blade as a function of time for the same parameter values as in Fig. 3; the solid curve is the result of the numerical computation and the dotted curve is the analytical prediction from Part I; the sudden jump in F_B coincides with the cutting of the vortex by the blade.

large angle of attack, however, the core radius is seen to increase substantially on one side and decrease on the other side of the aforementioned kink, which indicates that the vortex is stretched on one side of the kink and compressed on the other side. The variation of core radius becomes progressively steeper near the kink. Variation of vortex force on the blade with time is plotted in Fig. 10 for the two cases shown in Figs. 6 and 7, neither of which includes cutting of the vortex. It is clear from Fig. 10 that for large values of T/σ_o, a substantial variation of vortex force (and associated blade noise) occurs due to vortex bending alone, particularly at large angles of attack.

IV. Results for Vortex-Circular Cylinder Interactions

In the previous section, it was noted that the nature of the vortex response depends critically on whether the ratio of the

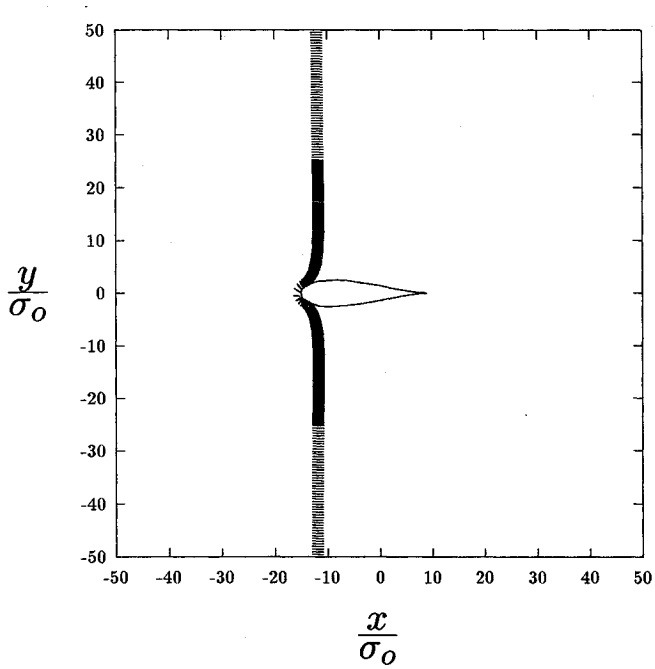

Fig. 6 Side view showing bending (prior to cutting) of a vortex with zero axial flow caused by interaction with a fairly thick blade, with $T/\sigma_o = 5$ and $2\pi U\sigma_o/\Gamma = 1$, at zero angle of attack.

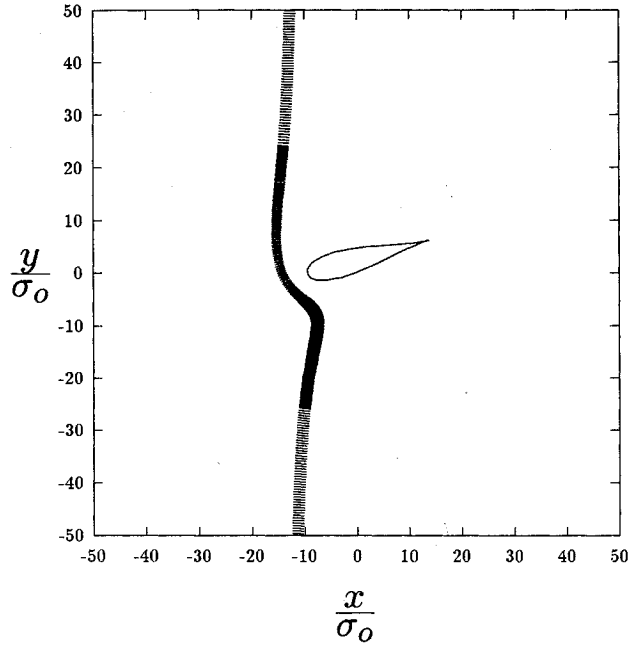

Fig. 7 Side view showing vortex deflection for a similar case to that shown in Fig. 6, but for a blade with angle of attack $\alpha = -15$ deg.

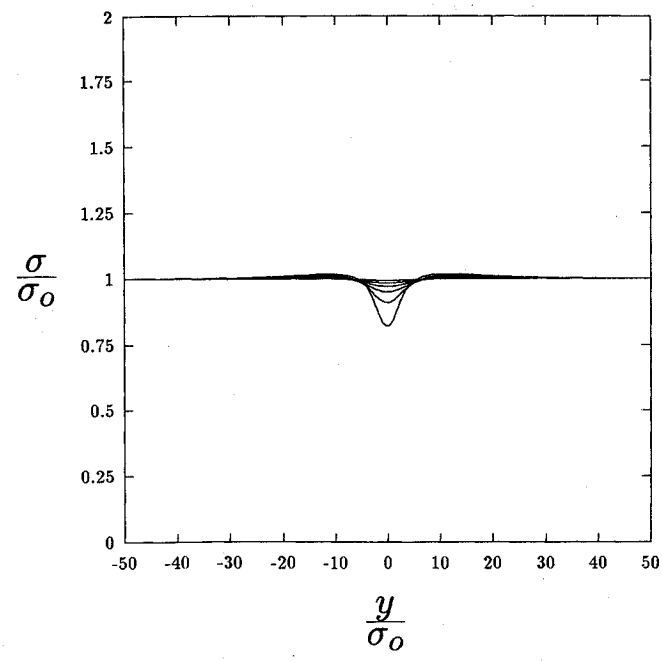

Fig. 8 Variation of vortex core radius σ with distance along the vortex for a series of times prior to cutting for the same case as in Fig. 6.

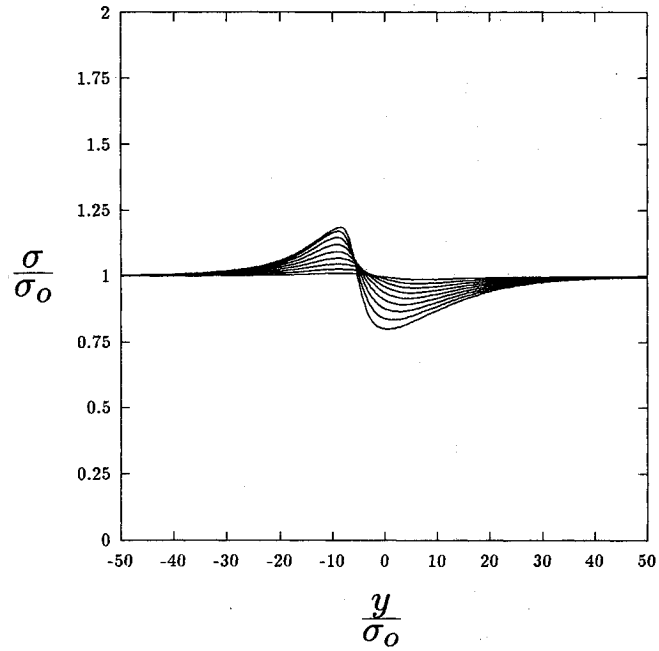

Fig. 9 Variation of vortex core radius σ with distance along the vortex for a series of times prior to cutting for the same case as in Fig. 7.

blade thickness to vortex core radius is large or small compared to unity. To isolate the effect of this parameter (as opposed to effects of blade angle of attack or chord, for instance), in the current section we present the results of computations on the interaction of a line vortex and a circular cylinder. As in the observations of the previous section, we find that the cylinder will enter the vortex (and subsequently cut the vortex) with very little vortex bending for values of D/σ_o less than or equal to 0(1), where D is the cylinder diameter. For D/σ_o greater than about 5, runs with different cylinder diameters all appear qualitatively similar, and the effect of the parameter $2\pi\sigma_o U/\Gamma$ is of primary importance.

For $D/\sigma_o \gg 1$, the general behavior of the vortex in response to the approach of a cylinder is illustrated in Fig. 11 (looking along the cylinder axis) for the case $D/\sigma_o = 10$ and

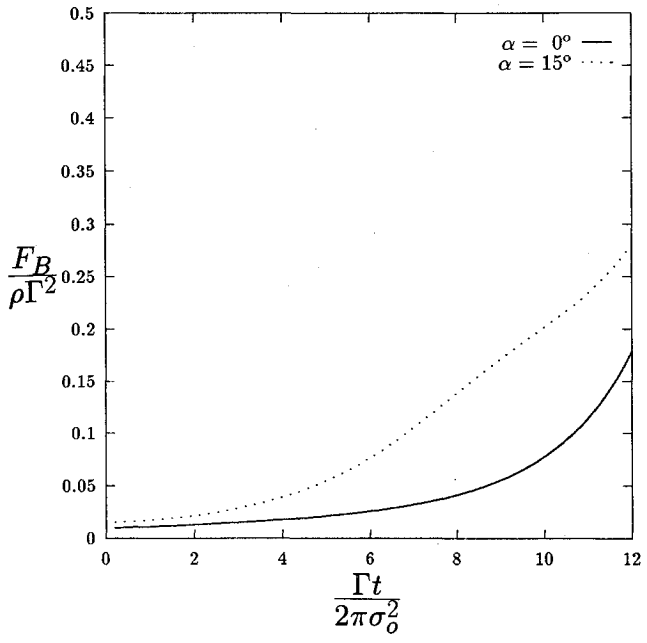

Fig. 10 Magnitude of the vortex force on the blade as a function of time (prior to cutting) for the two cases shown in Figs. 6 and 7, where the solid curve is for $\alpha = 0$ deg and the dotted curve is for $\alpha = 15$ deg.

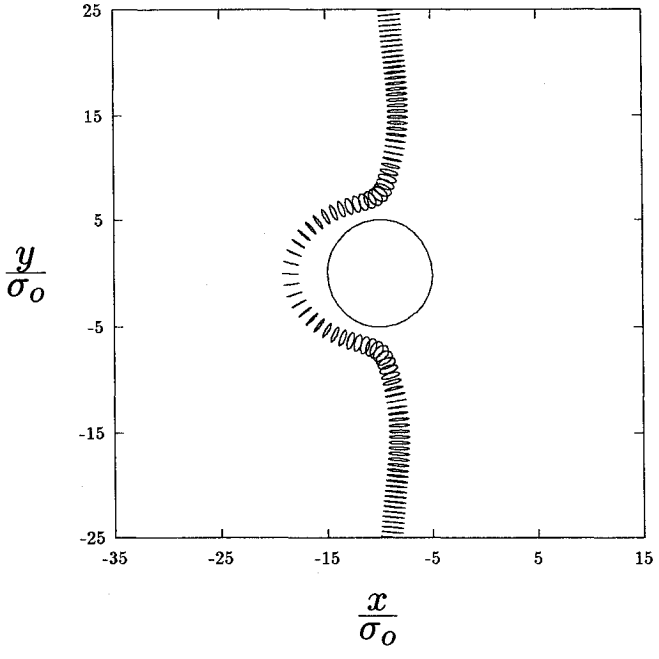

Fig. 11 Side view (looking down the cylinder axis) showing the bending of a vortex with no axial flow caused by interaction with a circular cylinder with diameter $D/\sigma_o = 10$ and forward speed $2\pi U\sigma_o/\Gamma = 1/2$.

$2\pi\sigma_o U/\Gamma = 1/2$, with no ambient axial flow. The vortex is observed to bend both away from the direction of motion of the cylinder and along the cylinder axis. The axial distance along the vortex which shows significant deflection from interaction with the cylinder has vertical length approximately equal to the cylinder diameter. In addition, except for very slow cylinder forward speeds, the minimum distance between the cylinder leading edge and the vortex seems to approach a nearly constant value as the cylinder approaches and passes through the vortex's initial position.

The deflection of the vortex axis for the same case as in Fig. 11 is shown for a series of times (plotted every 10 time steps) from two different views in Figs. 12a and 12b, which show the bending of the vortex both along the direction of the motion of the cylinder and in the spanwise direction. The variation of core radius and axial velocity along the vortex axis for this case is shown in Figs. 13a and 13b, such that the final curves drawn in Figs. 12 and 13 all correspond to the same times. The axial velocity is generated by a gradient in the core area and is directed upward in the lower half of the vortex and downward in the upper half, so as to refill the stretched part of the vortex core.

The decrease in vortex core radius near the cylinder leading edge is substantially more pronounced at higher cylinder forward speeds than at lower cylinder speeds at times with similar amounts of bending of the vortex in the direction of cylinder motion. An example of this behavior is shown in Fig. 14 via a plot of the core radius vs the vertical distance at a series of times (plotted every 5 time steps) for a case with $D/\sigma_o = 10$ and $2\pi\sigma_o U/\Gamma = 2$. Although the final curves in Figs. 13a and

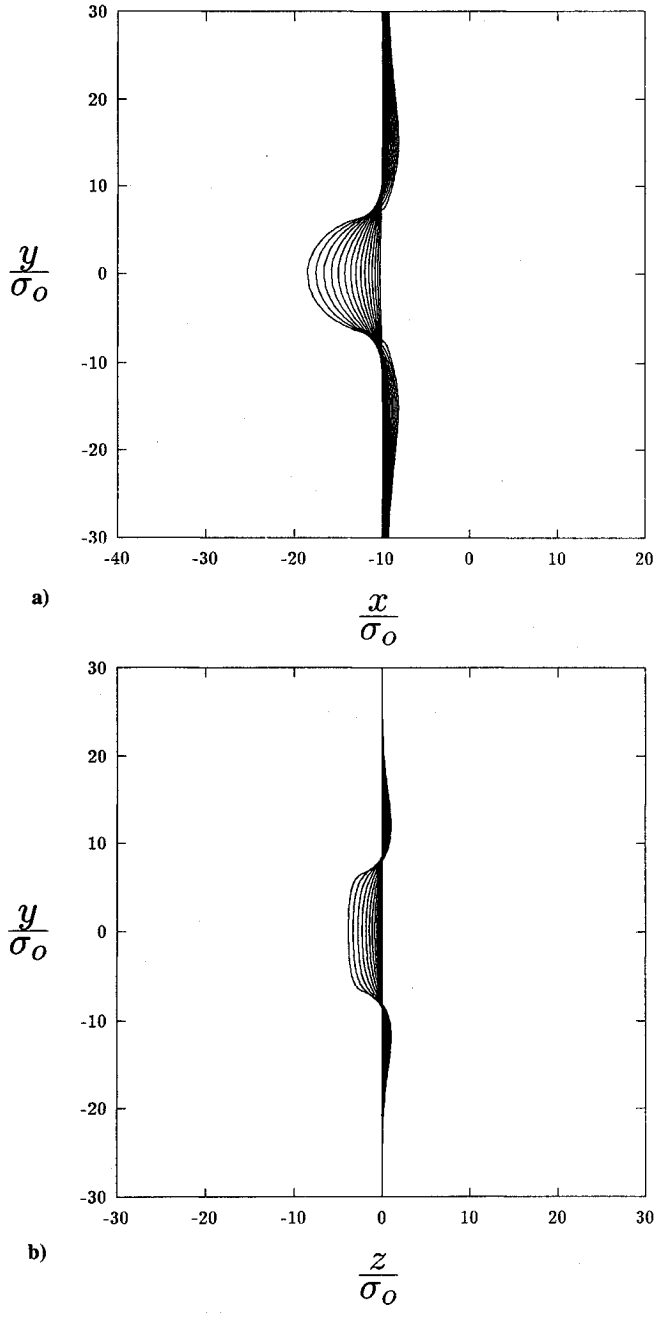

Fig. 12 Deflection of the vortex axis at a series of times for the same case as shown in Fig. 11: the view in a) is given looking along the cylinder axis (in the negative z direction) and the view in b) is given looking back along the direction of cylinder forward motion (in the positive x direction).

14 correspond to states with about the same amounts of vortex bending, the core radius decreases by nearly twice as much in the high-speed case shown in Fig. 14 as it does in the low-speed case shown in Fig. 13a. This observation is a consequence of the fact that for slower cylinder speeds the axial flow within the vortex (which is generated by axial variation in the core radius) has more time to partially refill the stretched portion of the vortex core. The deflection of the vortex along the cylinder axis is also much smaller for cases with high cylinder speed than it is for cases with low cylinder speed at equivalent amounts of vortex bending in the direction of the blade's forward motion.

For very low cylinder forward speeds, only a small amount of vortex bending occurs in the direction of cylinder motion until the cylinder leading edge comes very close to the vortex, at which point it is observed that the vortex bends towards the cylinder (opposite to the direction of cylinder motion) and eventually collapses onto the cylinder surface. An example of this behavior is shown in Fig. 15 for a case with $D/\sigma_o = 10$ and $2\pi\sigma_o U/\Gamma = 0.05$. This apparent attraction of the vortex

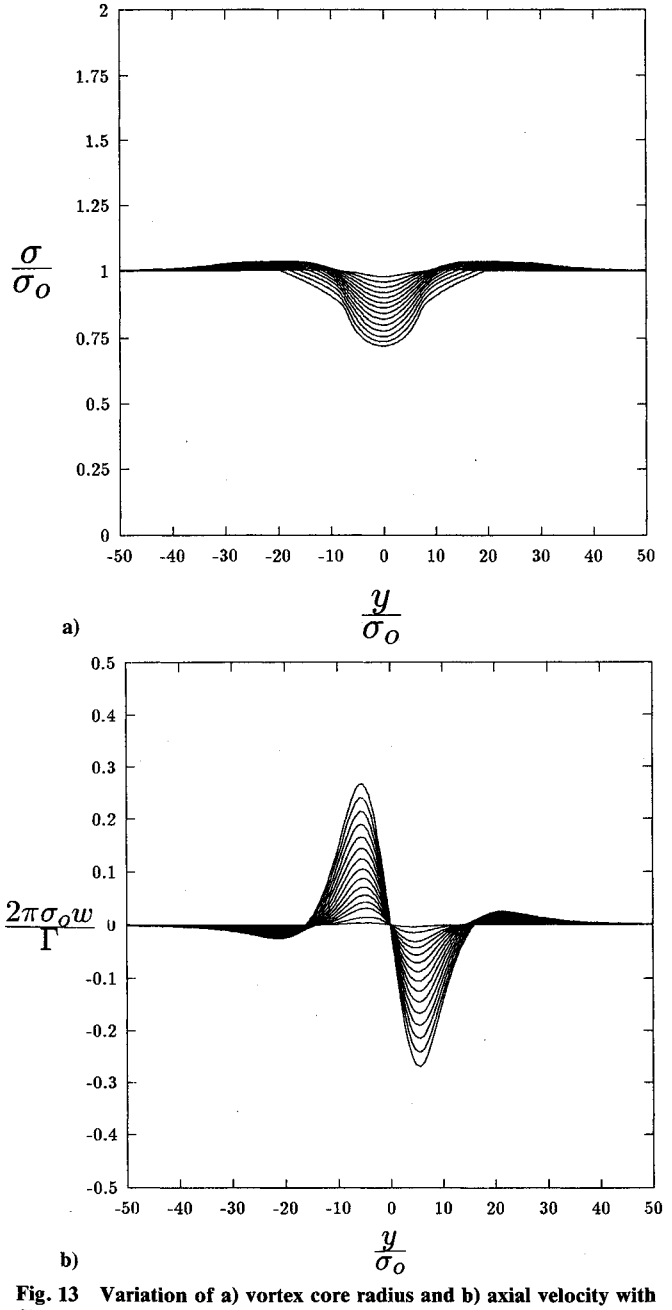

Fig. 13 Variation of a) vortex core radius and b) axial velocity with distance along the vortex axis at a series of times for the same case as in Fig. 11.

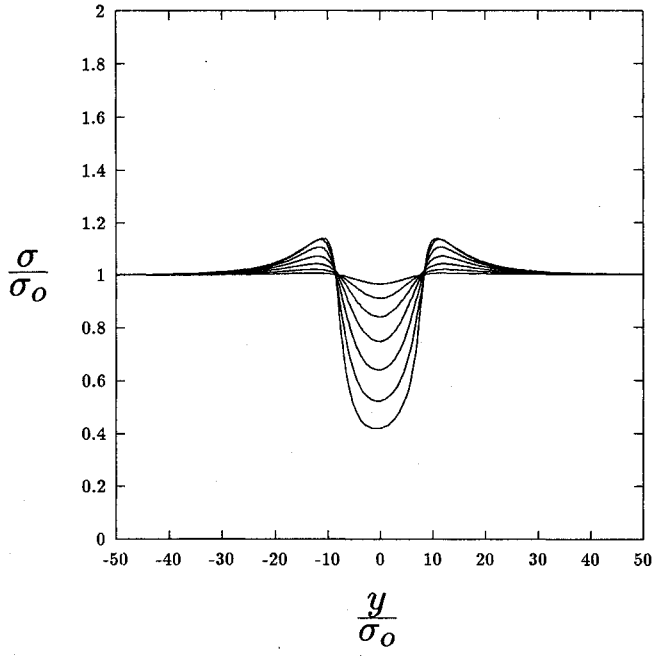

Fig. 14 Variation of vortex core radius with distance along the vortex axis at a series of times for a similar case to that shown in Fig. 11, but for a higher cylinder forward speed ($2\pi U\sigma_o/\Gamma = 2$); comparison of Figs. 13a and 14 shows the effect of cylinder forward speed on decrease in vortex core radius.

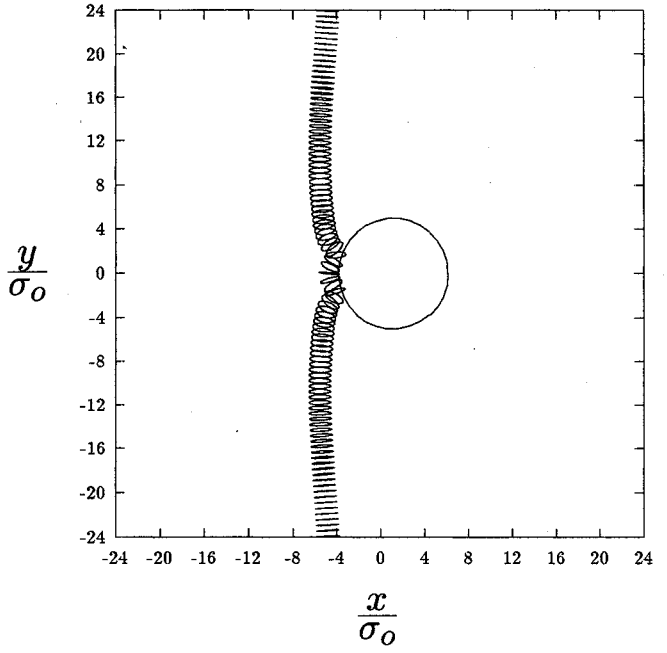

Fig. 15 Side view showing the attraction of the vortex to its image across the surface of the cylinder for a similar case to that shown in Fig. 11, but for a very slow forward speed ($2\pi U\sigma_o/\Gamma = 0.05$).

toward the cylinder seems to be a consequence of the self-induced velocity of the vortex due to the curvature of the vortex axis as it is deflected in the spanwise direction along the cylinder. For high cylinder speeds (i.e., larger values of $2\pi\sigma_o U/\Gamma$), the forward velocity imposed on the vortex by the cylinder motion would be sufficient to overcome the effect of vortex self-induced velocity, which leads to bending of the vortex away from the cylinder.

V. Conclusions

The computational results reported in this paper support the predictions of the analytical solution of the cutting of a

straight vortex by a blade obtained in Part I for sufficiently thin blades. The amount of vortex bending is found to depend strongly on the ratio T/σ_o of blade thickness to initial vortex core radius. For T/σ_o of order unity or less, there is very little vortex bending caused by interaction with the blade. For T/σ_o much greater than unity, the vortex will bend around the blade leading edge rather than be cut by the blade. In the case of thick blades (i.e., for large T/σ_o), the angle of attack and forward speed of the blade are found to have a substantial effect on the amount and nature of vortex deflection. We particularly note that thick blades with large angles of attack produce very substantial vortex bending, with the formation of a kink in the vortex that dominates the vortex behavior.

In the case of interaction of a vortex with a circular cylinder, we similarly find that substantial bending of the vortex will only occur for D/σ_o much greater than unity. For large D/σ_o, the amount of vortex bending increases with an increase in cylinder forward speed, and the bent section of the vortex is usually confined to a length along the vortex axis approximately equal to the cylinder diameter. The vortex diameter is observed to decrease in the stretched section near the cylinder leading edge, with substantially more decrease in core radius at higher cylinder forward speeds for a fixed amount of bending of the vortex axis. At low cylinder forward speeds, the vortex bends toward the cylinder and collapses onto the cylinder surface. This behavior is not observed at higher cylinder forward speeds, for which the vortex bends away from the cylinder. The qualitative form of the results presented here for vortex-circular cylinder interaction with large values of D/σ_o are similar to those obtained by Affes and Conlisk,[4] although we have included the effects of axial flow and variation in core radius. These effects become important for large values of $2\pi\sigma_o U/\Gamma$, for which the core radius varies substantially along the core due to stretching of the vortex by the cylinder (as shown, for instance, in Fig. 4).

With regard to the prediction of noise generation from normal blade-vortex interaction, we find that for thin blades (with T/σ_o of order unity or smaller) the present computational results support the proposition in Part I that variation in force on the blade (and hence the blade noise generation[10]) is dominated by vortex cutting and subsequent vortex shock and expansion wave formation, provided that the vortex force can be assumed to change monotonically from its value before cutting to its value after cutting. Here the rate of change of vortex force can be estimated from the jump in F_B during cutting divided by the time scale σ/U of cutting. The question of whether a spike in vortex force occurs during the actual cutting process cannot be investigated using a filament model, as was used in the present paper, and should be examined further.

For thick blades, such that T/σ_o is much larger than unity, the vortex behavior and subsequent impulsive sound generation will be dominated by bending and stretching, rather than cutting, of the vortex. Inviscid numerical calculations with vortex filament models that include a variable vortex core area, such as that described in the present paper, may provide an efficient means of estimating sound generation for thick blades, particularly if some means is provided for detecting breakup of the vortex when it comes in close proximity with the cylinder surface.

Acknowledgment

This work was supported by the U.S. Army Research Office under grant number DAAL03-92-G-0277. Supercomputer time on the Cray Y-MP at Florida State University was provided by a grant from the Florida Supercomputing Center. The authors wish to thank M. R. Dhanak for some helpful suggestions and A. Leonard for suggesting an explanation for the vortex response shown in Fig. 15.

References

[1]Marshall, J. S., "Vortex Cutting by a Blade, Part I: General Theory and a Simple Solution," *AIAA Journal,* Vol. 32, No. 6, pp. 1145–1150.

[2]Dhanak, M. R., "Interaction Between a Vortex Filament and an Approaching Rigid Sphere," *Journal of Fluid Mechanics,* Vol. 110, Sept. 1981, pp. 129–147.

[3]Pedrizzetti, G., "Close Interaction Between a Vortex Filament and a Rigid Sphere," *Journal of Fluid Mechanics,* Vol. 245, Dec. 1992, pp. 701–722.

[4]Affes, H. and Conlisk, A. T., "A Simplified Model for the Interaction of a Rotor Tip Vortex with an Airframe," AIAA Paper 92-0320, Jan. 1992.

[5]Liou, S. G., Komerath, N. M., and McMahon, H. M., "Measurement of the Interaction Between a Rotor Tip Vortex and a Cylinder," *AIAA Journal,* Vol. 28, No. 6, 1990, pp. 975–981.

[6]Lewis, R. I., *Vortex Element Methods for Fluid Dynamic Analysis of Engineering Systems,* Cambridge Univ. Press, Cambridge, England, UK, 1991, Chaps. 1 and 2.

[7]Peyret, R., and Taylor, T. D., *Computational Methods for Fluid Flow,* Springer-Verlag, New York, 1983, pp. 104–105.

[8]Yalamanchili, R., "Computations of Normal Vortex Interaction with Blades and Circular Cylinders," M.S. Thesis, Dept. of Ocean Engineering, Florida Atlantic Univ., Boca Raton, FL, Dec. 1993.

[9]Dhanak, M. R., and DeBernardinis, B., "The Evolution of an Elliptical Vortex Ring," *Journal of Fluid Mechanics,* Vol. 109, Aug. 1981, pp. 189–216.

[10]Howe, M. S., "On Unsteady Surface Forces, and Sound Produced by the Normal Chopping of a Rectilinear Vortex," *Journal of Fluid Mechanics,* Vol. 206, Sept. 1989, pp. 131–153.